



Supplement of

Contribution of combustion Fe in marine aerosols over the northwestern Pacific estimated by Fe stable isotope ratios

Minako Kurisu et al.

Correspondence to: Minako Kurisu (kurisum@jamstec.go.jp)

The copyright of individual parts of the supplement might differ from the article licence.

Table S1: Aerosol sampling periods of KH-13-7 cruise. Solar radiation flux is the average flux along the backward trajectory calculated by the HYSPLIT model (Stein et al., 2015).

No.	Start time (UTC)	Start point	Total Flow (m ³)	Solar radiation flux (W m ⁻²)
			End time (UTC)	End point
13-a	12 Dec, 11:04 p.m.	29.22° N, 147.92° E	923.14	149.7
	15 Dec, 10:00 p.m.	20.00° N, 160.00° E		
13-b	15 Dec, 10:05 p.m.	20.00° N, 160.00° E	717.09	243.3
	18 Dec, 9:01 p.m.	11.80° N, 172.28° E		
13-c	2 Feb, 10:12 p.m.	3.67° N, 159.44° E	734.02	256.3
	5 Feb, 11:05 p.m.	19.39° N, 150.31° E		
13-d	5 Feb, 11:08 p.m.	19.39° N, 150.31° E	605.99	158.5
	9 Feb, 0:03 a.m.	29.62° N, 142.33° E		
13-e	9 Feb, 0:05 a.m.	29.62° N, 142.33° E	597.42	122.7
	11 Feb, 0:03 a.m.	35.17° N, 139.77° E		

Table S2. Aerosol sampling periods of KH-14-3 cruise. Solar radiation flux is the average flux along the backward trajectory calculated by the HYSPLIT model (Stein et al., 2015).

No.	Start time (UTC)	Start point	Total Flow (m ³)	Solar radiation
	End time (UTC)	End point		flux (W m ⁻²)
14-A	24 June, 0:13 a.m.	32.40° N, 143.09° E	710.64	386.9
	26 June, 10:04 p.m.	22.00° N, 157.26° E		
14-B	26 June, 10:06 a.m.	22.00° N, 157.26° E	468.72	376.3
	28 June, 1:08 p.m.	17.56° N, 163.05° E		
14-C	30 June, 10:04 p.m.	10.33° N, 174.18° E	887.42	345.7
	3 July, 8:00 p.m.	1.24° N, 171.45° W		
14-D	3 July, 8:04 p.m.	1.24° N, 171.45° W	818.32	331.4
	6 July, 7:55 p.m.	10.02° N, 170.02° W		
14-E	6 July, 7:57 p.m.	10.02° N, 170.02° W	864.71	381.7
	9 July, 8:20 p.m.	20.01° N, 169.57° W		
14-F	9 July, 8:22 p.m.	20.01° N, 169.57° W	871.97	390.3
	12 July, 6:59 p.m.	20.46° N, 161.33° W		
14-G	12 July, 7:02 p.m.	20.46° N, 161.33° W	228.41	390.5
	13 July, 3:57 p.m.	21.01° N, 157.59° W		
14-H	18 July, 4:13 a.m.	21.51° N, 157.36° W	345.16	392.2
	20 July, 8:01 p.m.	30.02° N, 170.01° W		
14-I	20 July, 8:03 p.m.	30.02° N, 170.01° W	898.01	391.3
	23 July, 7:58 p.m.	40.03° N, 171.00° W		
14-J	23 July, 8:00 p.m.	40.03° N, 171.00° W	933.27	383.5
	26 July, 8:00 p.m.	50.02° N, 169.56° W		
14-K	26 July, 8:02 p.m.	50.02° N, 169.56° W	944.25	371.2
	29 July, 8:57 p.m.	63.38° N, 167.38° W		
14-L	29 July, 9:01 p.m.	63.38° N, 167.38° W	748.4	364.4
	1 Aug, 8:59 p.m.	60.44° N, 176.03° W		
14-M	1 Aug, 9:00 p.m.	60.44° N, 176.03° W	954.26	371.4
	4 Aug, 9:57 p.m.	47.39° N, 167.08° E		
14-N	4 Aug, 10:00 p.m.	47.39° N, 167.08° E	926.04	377.0
	8 Aug, 0:05 a.m.	37.33° N, 145.15° E		
14-O	8 Aug, 0:07 a.m.	37.33° N, 145.15° E	293.43	375.8
	8 Aug, 11:59 p.m.	35.26° N, 139.48° E		

Table S3. Comparison of elemental concentrations ($\mu\text{g/g}$) of CJ-2 (Simulated Asian mineral dust) measured in this study ($\pm\text{SD}$, $n=3$) and Nishikawa et al. (2000).

	Ti	V	Fe	Pb
measured value ($\pm\text{SD}$)	4400 \pm 110	67.4 \pm 18.4	29600 \pm 2500	21.3 \pm 6.2
Nishikawa et al. (2000)	4600	77	30200	21.2

Table S4. The flow of Fe separation with the anion exchange resin.

Objective	Solution	Volume per each introduction [µL]	Repetition
1. Rinse	6 M HCl	250	4
2. Rinse	UPW	60	5
3. Conditioning	6 M HCl/0.3 mM H ₂ O ₂	200	1
4. Sample introduction	Sample in 6 M HCl/0.3 mM H ₂ O ₂	200	1
5. Elution of Cu, Cr	6 M HCl/0.3 mM H ₂ O ₂	30	14
6. Elution of Fe	1 M HCl/0.3 mM H ₂ O ₂	30	12

Table S5. Atmospheric Fe concentrations and isotope ratios of total (acid-digested) and soluble Fe of the KH-13-7 samples. n.a.: not available due to small quantity of sample Fe or high filter blank.

No. (Group)	Coarse			Fine			Bulk (Coarse+Fine)
	Fe conc. (ng m ⁻³) *	$\delta^{56}\text{Fe} \pm 2\text{SE} (\text{\textperthousand})$ **		Fe conc. (ng m ⁻³) **	$\delta^{56}\text{Fe} \pm 2\text{SE} (\text{\textperthousand})$ **		$\delta^{56}\text{Fe} \pm 2\text{SE} (\text{\textperthousand})$
		Total	Soluble		Total	Soluble	
13-a (I)	8.07 (0.1 %)*	-0.06±0.14 (-0.11±0.13)**	n.a.	4.70 (4 %)	-1.46±0.22 (-1.34±0.21)	n.a.	-0.58±0.12
13-b (II)	0.47 (2 %)	0.10±0.25 (0.09±0.24)	n.a.	0.54 (29 %)	-0.01±0.23 (0.02±0.22)	n.a.	0.04±0.17
13-c (II)	1.28 (1 %)	0.38±0.28 (0.38±0.26)	n.a.	0.77 (22 %)	0.15±0.20 (0.02±0.22)	n.a.	0.30±0.19
13-d (I)	14.64 (0.1 %)	0.03±0.18 (0.02±0.16)	n.a.	4.15 (6 %)	-0.45±0.28 (-0.42±0.27)	-2.23±0.04	-0.07±0.15
13-e (I)	22.72 (0.1 %)	0.10±0.14 (0.08±0.13)	-0.27±0.03	11.09 (2 %)	-0.47±0.18 (-0.46±0.16)	-1.14±0.03	-0.09±0.11

*Fe concentrations were calculated after subtraction of blank concentration. Fraction of Fe in blank filter to sample filter is shown in the parenthesis.

** $\delta^{56}\text{Fe}$ values before the correction of blank filter is shown in the parenthesis.

Table S6. Atmospheric Fe concentrations and isotope ratios of total (acid-digested) Fe of the KH-14-3 samples.

<D.L.: under detection limit (approximately <0.01 ng m⁻³ and <0.2 ng m⁻³ for coarse and fine particles, respectively), n.a.: not available due to small quantity of sample Fe or high filter blank.

No. (Group)	Coarse		Fine		Bulk (Coarse+Fine)
	Fe conc. (ng m ⁻³)*	$\delta^{56}\text{Fe} \pm 2\text{SE} (\text{\textperthousand})$ **	Fe conc. (ng m ⁻³)*	$\delta^{56}\text{Fe} \pm 2\text{SE} (\text{\textperthousand})$ **	$\delta^{56}\text{Fe} \pm 2\text{SE} (\text{\textperthousand})$
	Total		Total		Total
14-A (I)	1.54 (1 %)	n.a.	1.07 (23 %)	-0.64±0.15 (-0.41±0.13)	n.a.
14-B (II)	0.62 (3 %)	0.06±0.18 (0.09±0.16)	1.20 (29 %)	0.41±0.14 (0.31±0.12)	0.29±0.11
14-C (II)	0.98 (1 %)	0.43±0.11 (0.42±0.08)	0.46 (36 %)	0.39±0.12 (0.31±0.10)	0.42±0.08
14-D (II)	0.13 (8 %)	n.a.	0.46 (38 %)	n.a.	n.a.
14-E (II)	0.91 (1 %)	0.28±0.10 (0.26±0.08)	0.78 (26 %)	0.02±0.15 (0.05±0.13)	0.16±0.09
14-F (II)	1.11 (1 %)	0.36±0.15 (0.35±0.14)	0.35 (43 %)	0.17±0.15 (0.16±0.14)	0.32±0.12
14-G (II)	2.31 (2 %)	0.37±0.26 (0.37±0.25)	1.75 (36 %)	0.43±0.10 (0.34±0.07)	0.39±0.15
14-H (II)	4.58 (1 %)	0.18±0.11 (0.17±0.09)	0.72 (28 %)	n.a.	n.a.
14-I (II)	0.29 (4 %)	0.05±0.32 (0.06±0.31)	< D.L.	n.a.	n.a.
14-J (III)	1.30 (1 %)	0.09±0.14 (0.09±0.12)	< D.L.	n.a.	n.a.
14-K (III)	2.72 (0.4 %)	0.07±0.11 (0.07±0.09)	< D.L.	n.a.	n.a.
14-L (III)	0.45 (3 %)	0.31±0.14 (0.31±0.12)	0.54 (36 %)	0.43±0.17 (0.30±0.16)	0.37±0.11
14-M (III)	2.10 (0.5 %)	0.09±0.10 (0.09±0.07)	< D.L.	n.a.	n.a.
14-N (I)	4.15 (1 %)	0.07±0.29 (-0.04±0.28)	4.94 (20 %)	-1.45±0.23 (-1.17±0.22)	-0.76±0.18
14-O (I)	27.16 (1 %)	-0.24±0.24 (-0.30±0.23)	14.63 (13 %)	-2.16±0.30 (-1.72±0.29)	-0.91±0.19

*Fe concentrations were calculated after subtraction of blank concentration. Fraction of Fe in blank filter to sample filter is shown in the parenthesis.

** $\delta^{56}\text{Fe}$ values before the correction of blank filter is shown in the parenthesis.

Table S7. The fraction (%) of each Fe species estimated by the linear combination fitting of XANES spectra.
n.a.: not available due to small quantity of sample Fe or high filter blank.

No.	Coarse			Fine		
	Fe-containing aluminosilicates	Fe (hydr)oxides	R	Fe-containing aluminosilicates	Fe (hydr)oxides	R
13-a	59	41	0.013	34	66	0.012
13-b	55	45	0.026	43	57	0.028
13-c	21	79	0.013	20	80	0.029
13-d	42	58	0.012	32	68	0.012
13-e	66	34	0.013	52	48	0.017
14-A	37	63	0.014	42	58	0.021
14-B	77	23	0.022	33	67	0.029
14-C	40	60	0.016	36	64	0.044
14-D	n.a.			n.a.		
14-E	35	65	0.011	27	73	0.028
14-F	36	64	0.015	33	67	0.029
14-G	52	48	0.040	44	56	0.028
14-H	56	44	0.008	24	76	0.017
14-I	82	18	0.011	n.a.		
14-J	21	79	0.013	n.a.		
14-K	23	77	0.015	n.a.		
14-L	27	73	0.014	n.a.		
14-M	36	64	0.022	n.a.		
14-N	54	46	0.020	36	64	0.019
14-O	35	65	0.018	12	88	0.054

Table S8. Total and soluble Fe deposition flux of natural and combustion Fe.

	Total Fe deposition flux (nmol m ⁻² day ⁻¹)		Soluble Fe deposition flux (nmol m ⁻² day ⁻¹)	
	Natural Fe	Combustion Fe	Natural Fe	Combustion Fe
group I	291	15	2.9	1.4
II	27	0	0.2	0
III	32	0	0.4	0

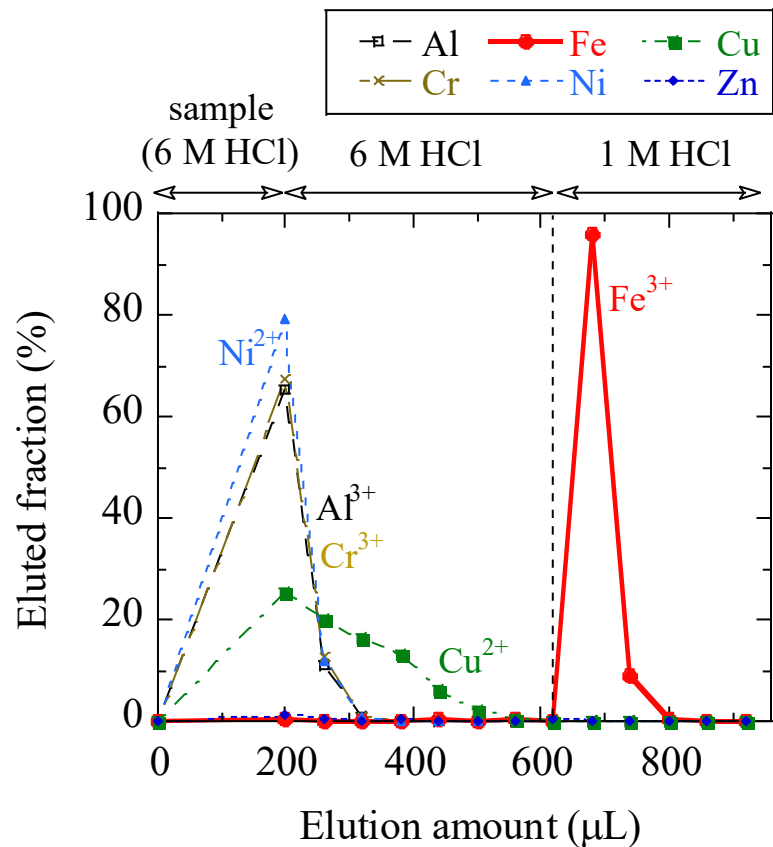


Figure S1. Elution curves of Al³⁺, Cr³⁺, Fe³⁺, Ni²⁺, and Cu²⁺ with the anion exchange resin.

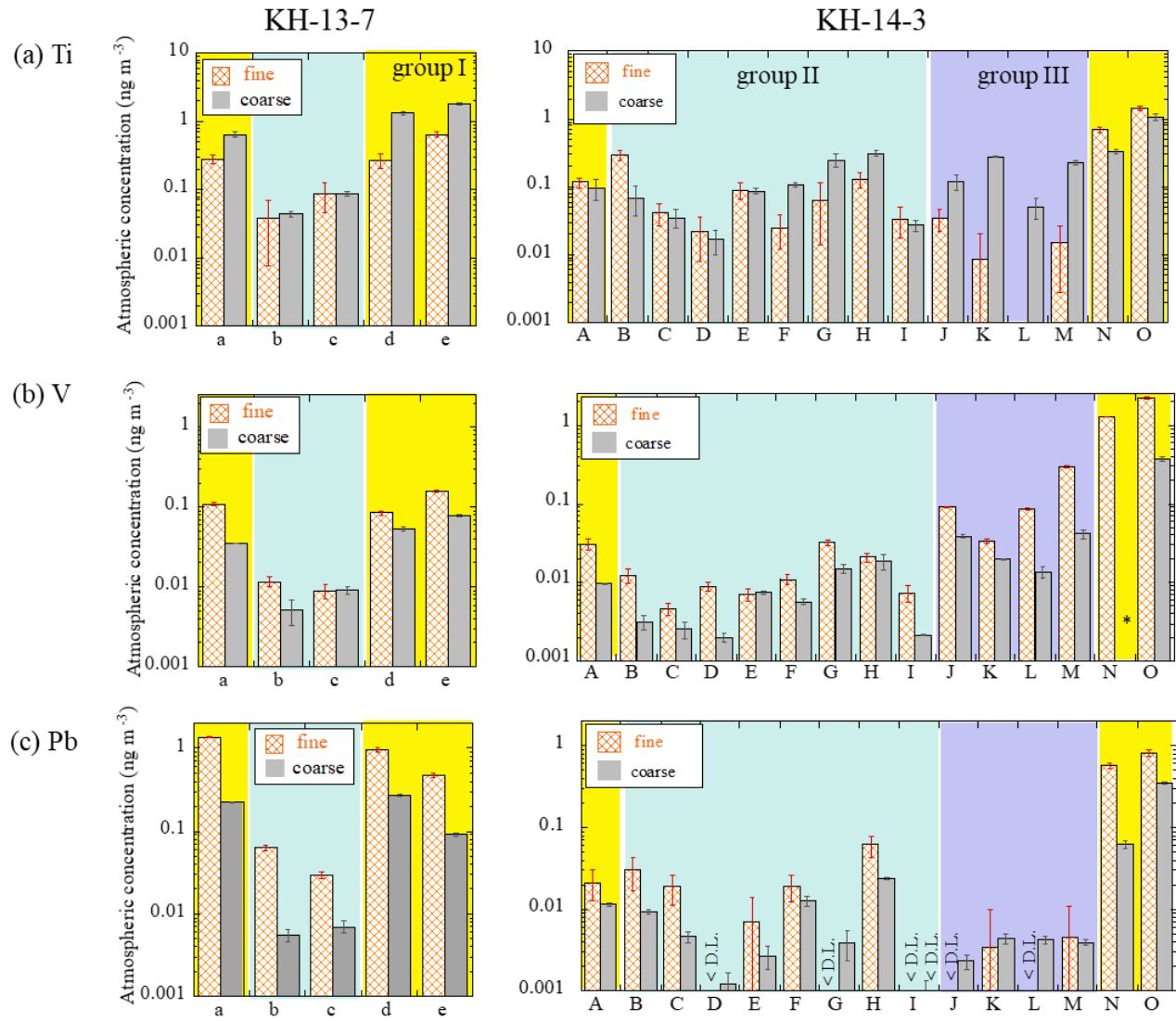


Figure S2. Atmospheric concentrations of (a) Ti, (b) V, and (c) Pb in size fractionated aerosols collected during KH-13-7 and KH-14-3 cruises. Errors are calculated from ICP-MS error and blank subtraction error. Yellow, blue, and purple areas indicate the group I (air masses from the Asian continent), II (air masses from the central and eastern Pacific), and III (air masses from the northern North Pacific), respectively. <D.L.: under detection limit due to higher concentrations in blank than samples.

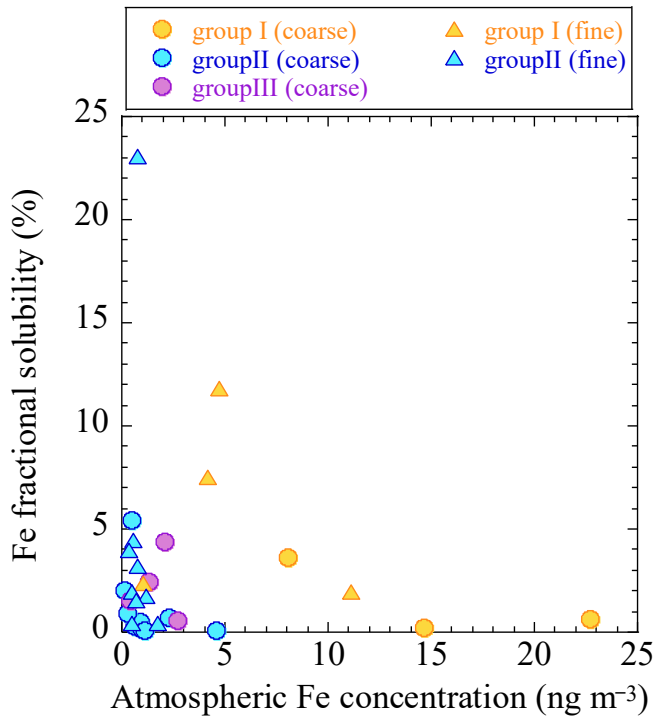


Figure S3. Scatter plot of atmospheric Fe concentration vs. Fe fractional solubility.

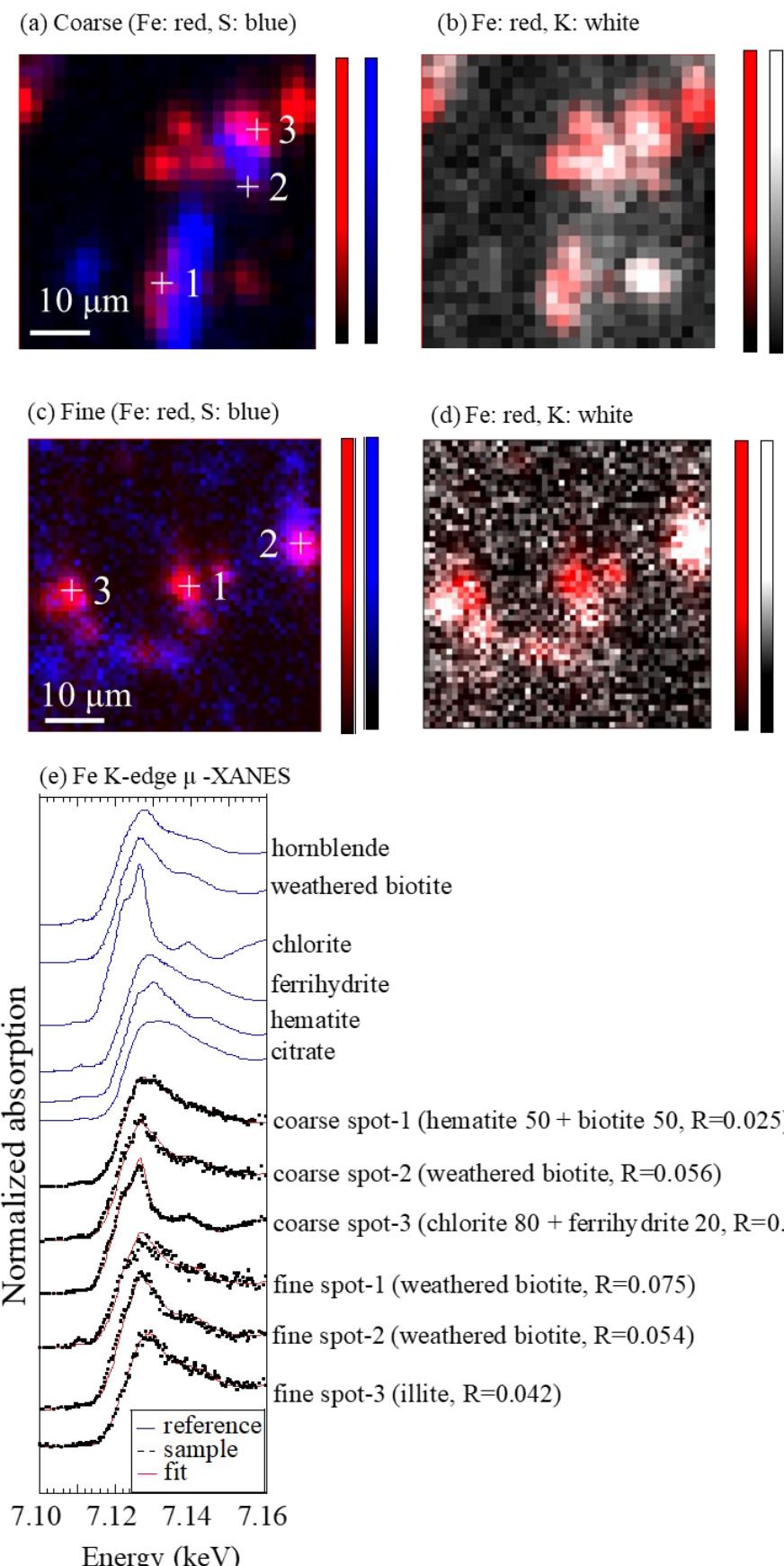
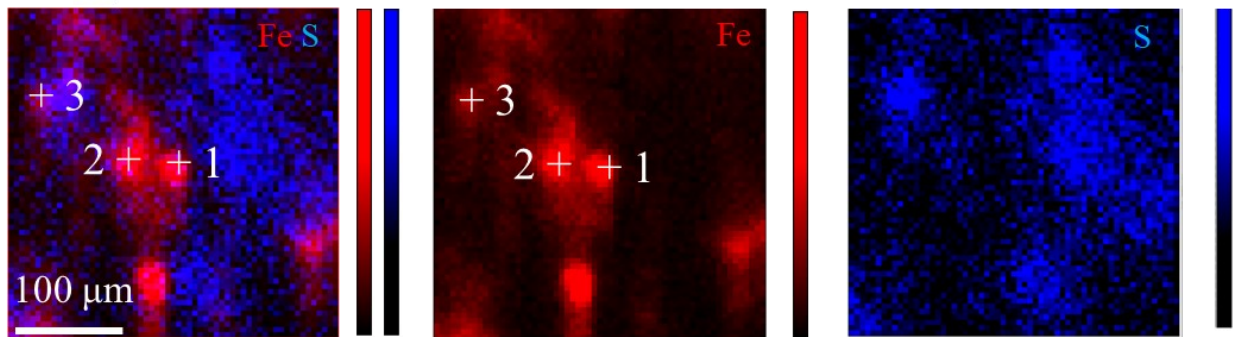
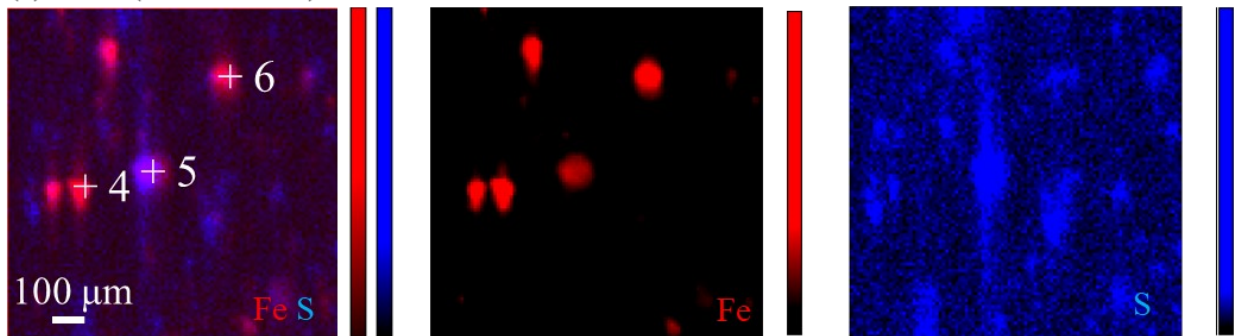


Figure S4. μ -XRF maps of Fe, S, and K in (a,b) coarse and (c,d) fine particles of 13-a. (e) μ -XANES spectra of the points in (a)-(d).

(a) Area I (Fe: red, S: blue)



(b) Area II (Fe: red, S: blue)



(c) Fe K-edge μ -XANES

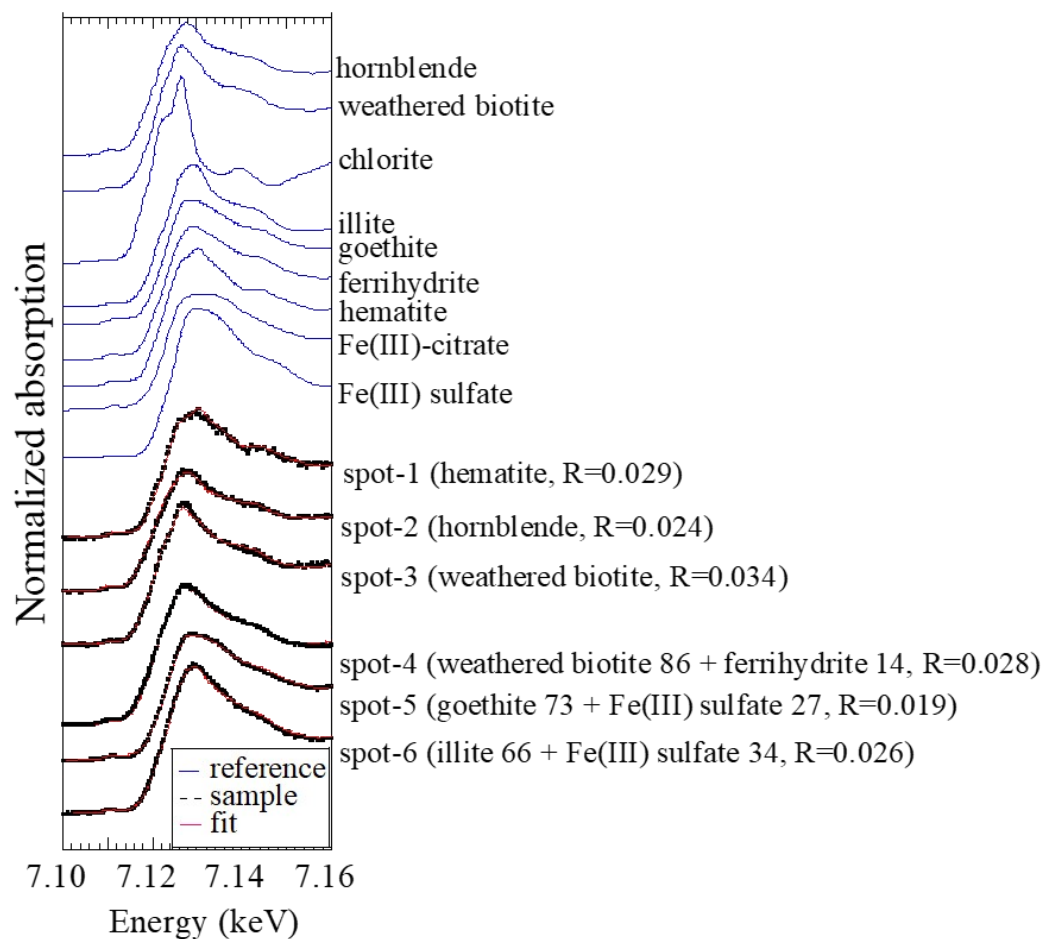


Figure S5. (a,b) μ -XRF maps of Fe and S in coarse particles of 13-c. (c) μ -XANES spectra of the points in (a-f).

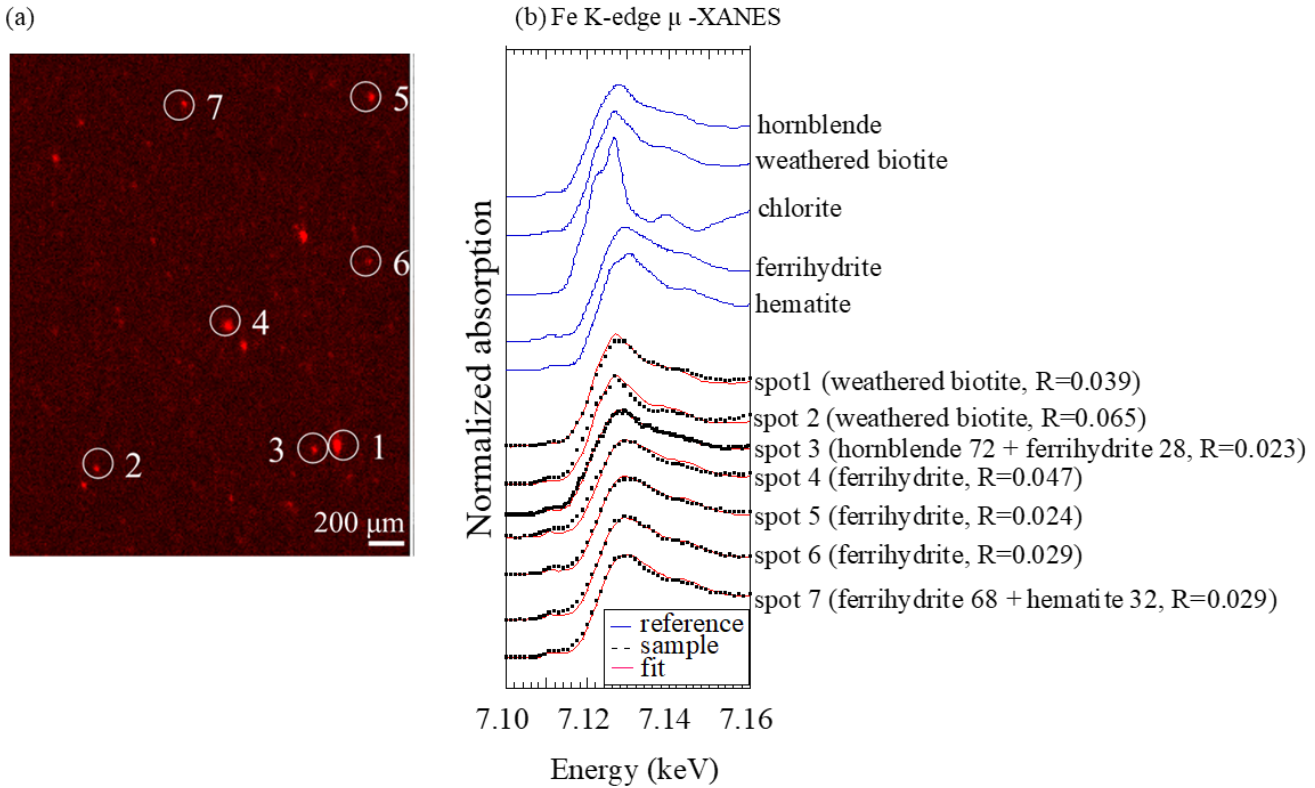


Figure S6. (a) μ -XRF maps of Fe in fine particles of 13-c. (b) μ -XANES spectra of the points in (a).

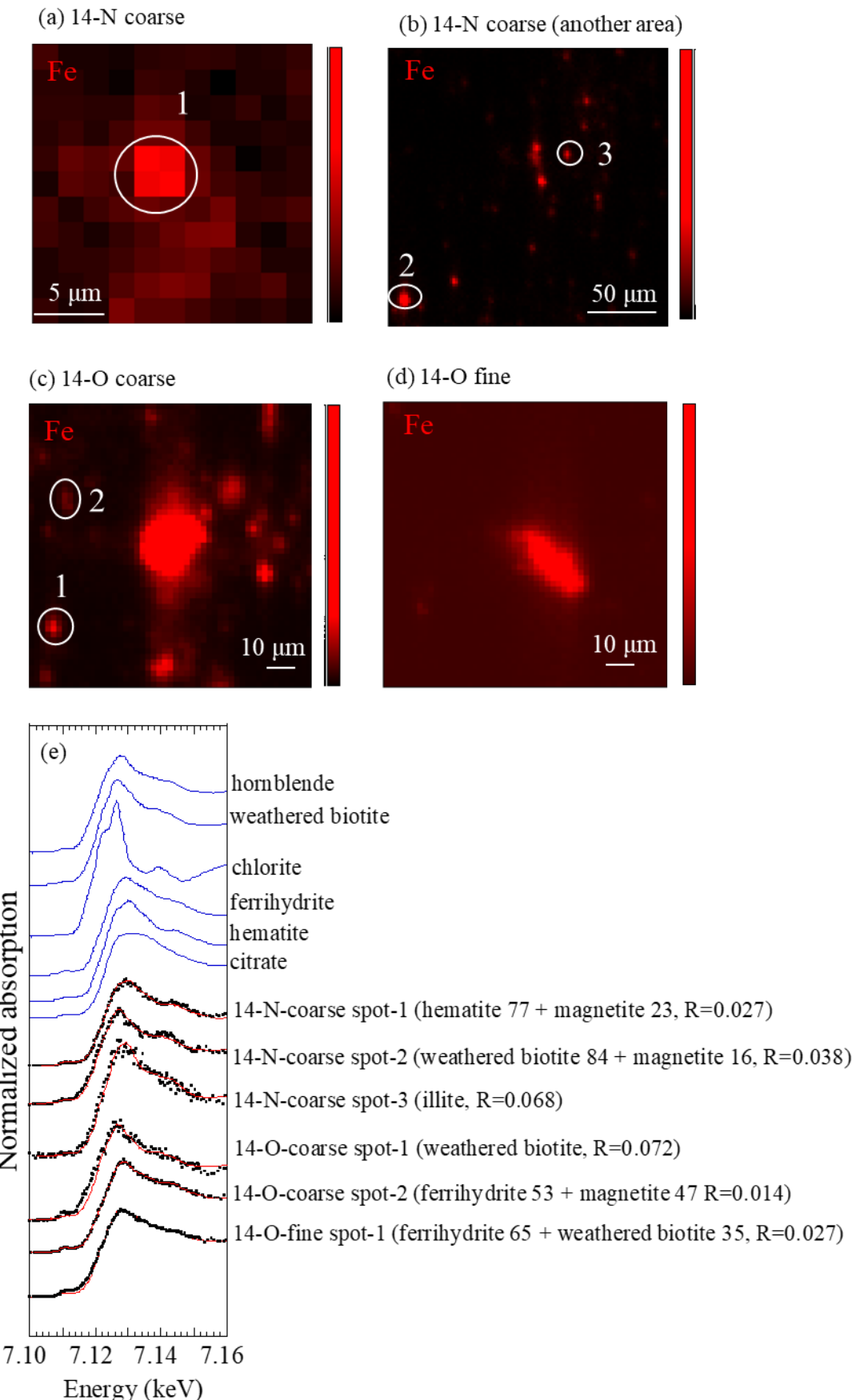


Figure S7. μ -XRF maps of Fe in (a, b) coarse particles of 14-N, (c) coarse particles of 14-O, and (d) fine particles of 14-O. (e) μ -XANES spectra of the points in (a-d).

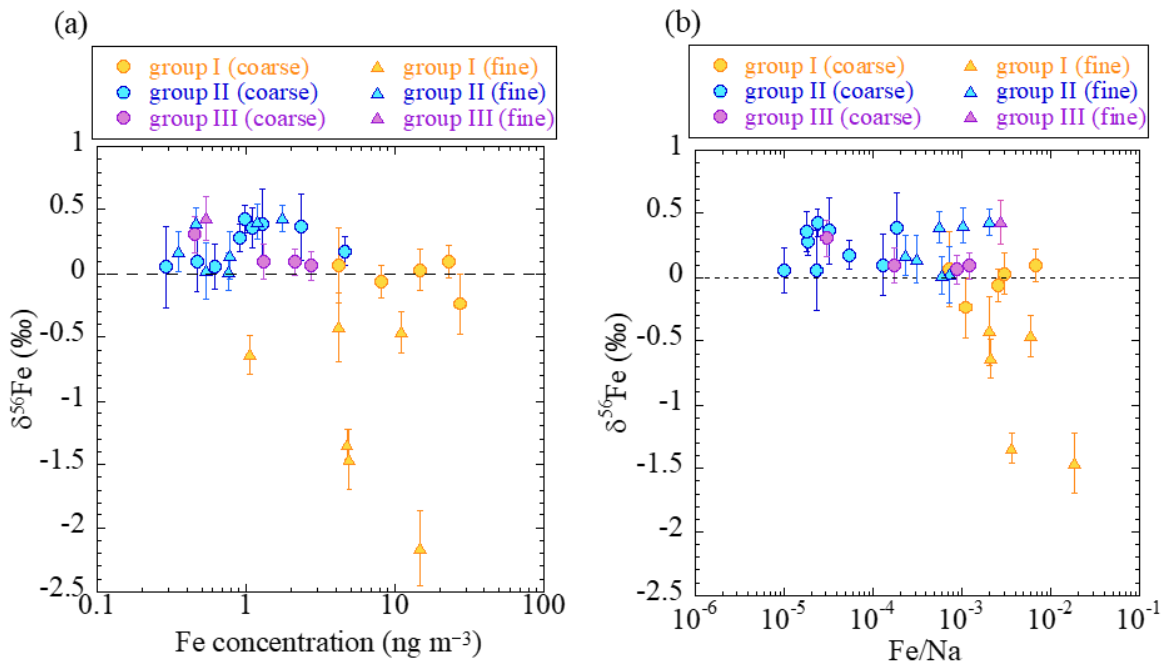


Figure S8. The relationship between (a) the atmospheric Fe concentration and $\delta^{56}\text{Fe}$ and (b) Fe/Na molar ratio and $\delta^{56}\text{Fe}$. Na data were obtained from Sun et al. (2017). Note that the Fe/Na in surface seawater is 10^{-10} - 10^{-8} .

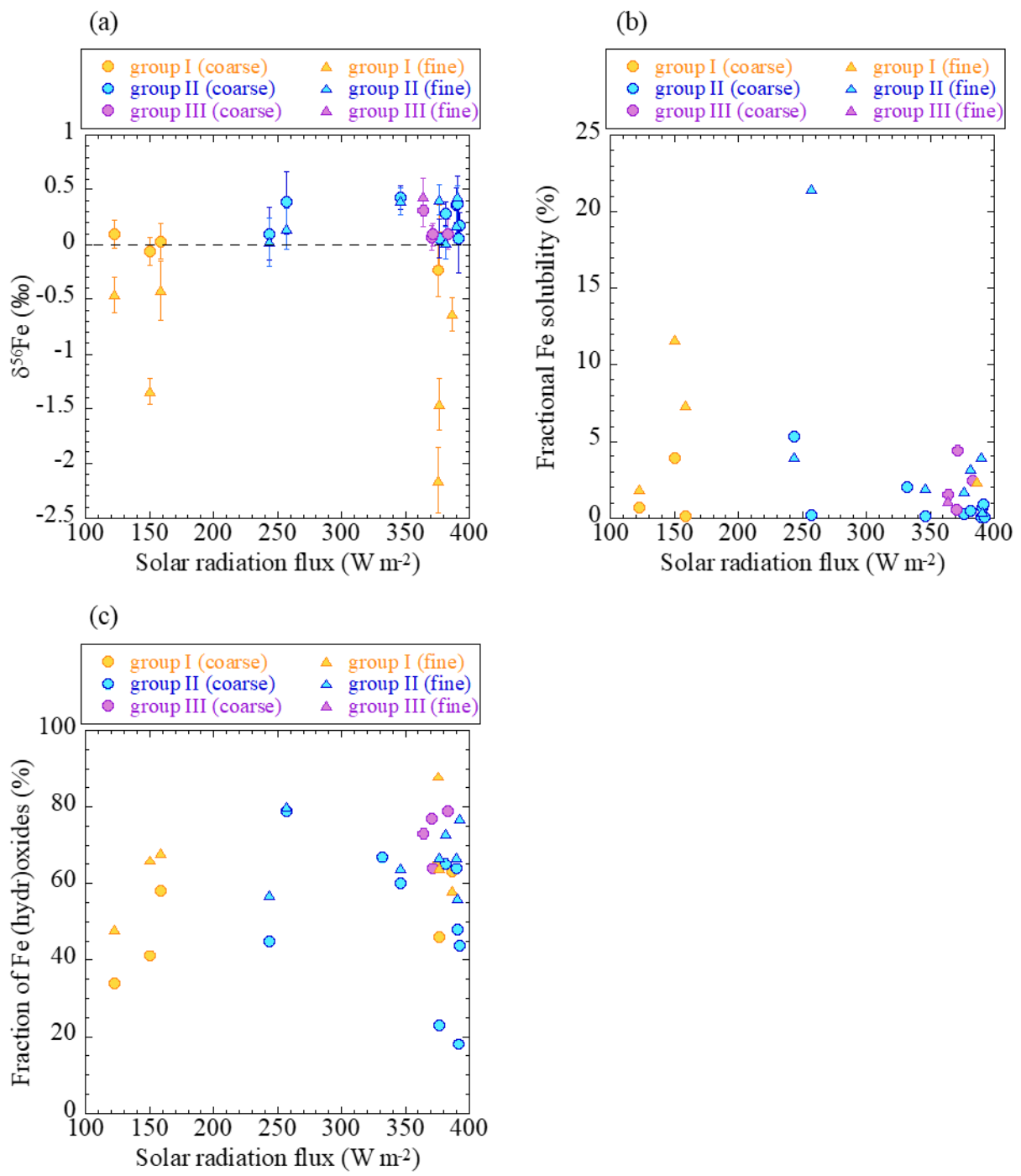


Figure S9. The relationship between the average solar radiation flux and (a) $\delta^{56}\text{Fe}$, (b) fractional Fe solubility, and (c) fraction of Fe (hydr)oxides. Yellow: group I; blue: group II; purple: group III.

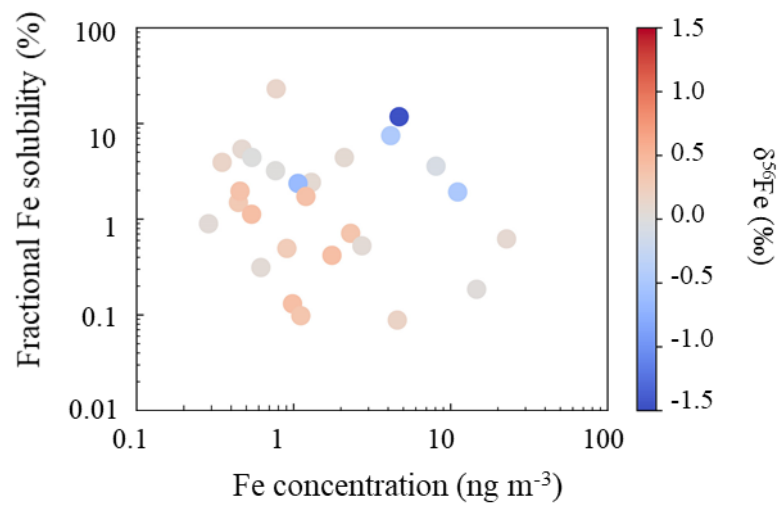


Figure S10. The relationship between the atmospheric Fe concentration and the fractional Fe solubility. The color scale indicates $\delta^{56}\text{Fe}$.

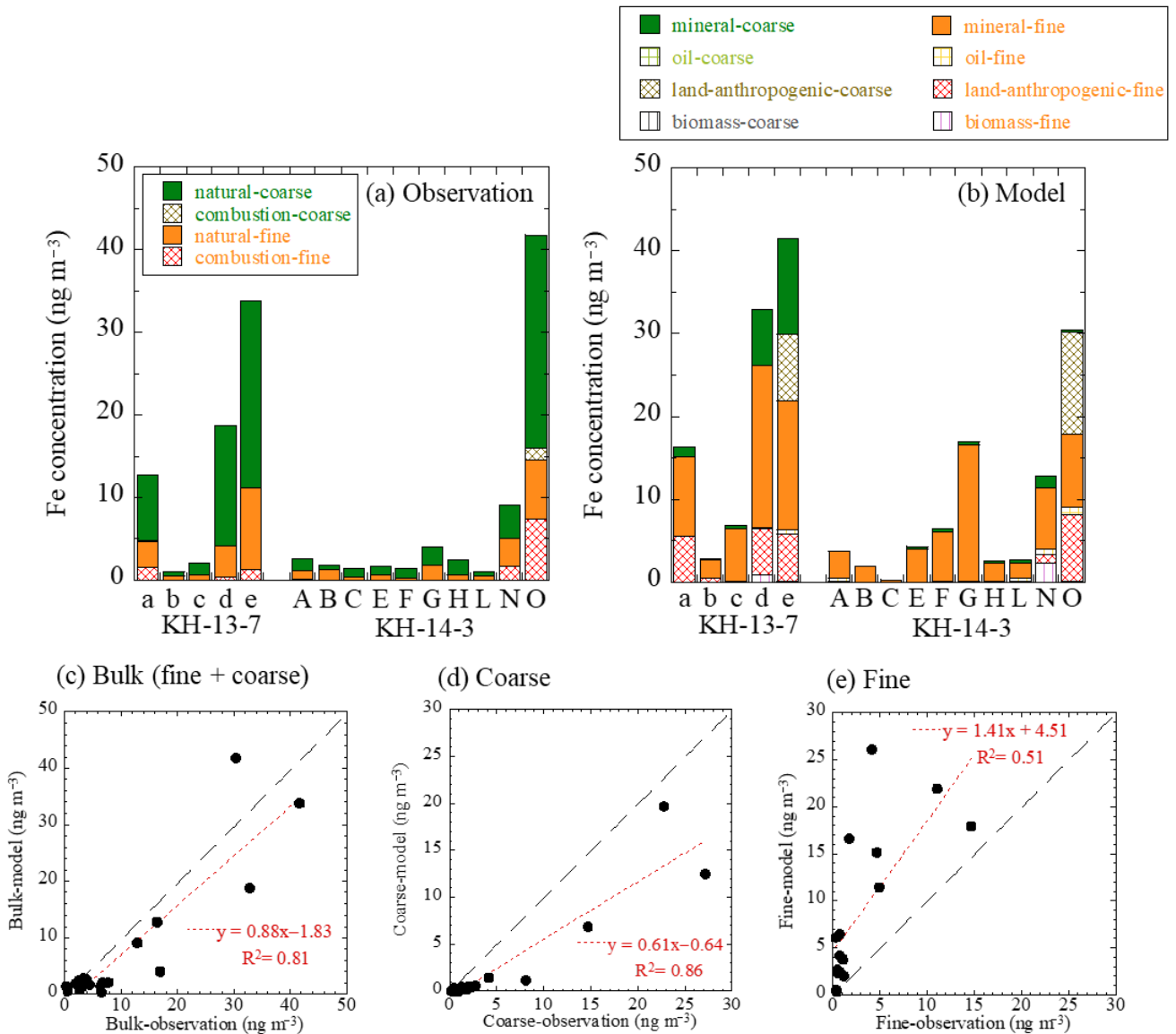
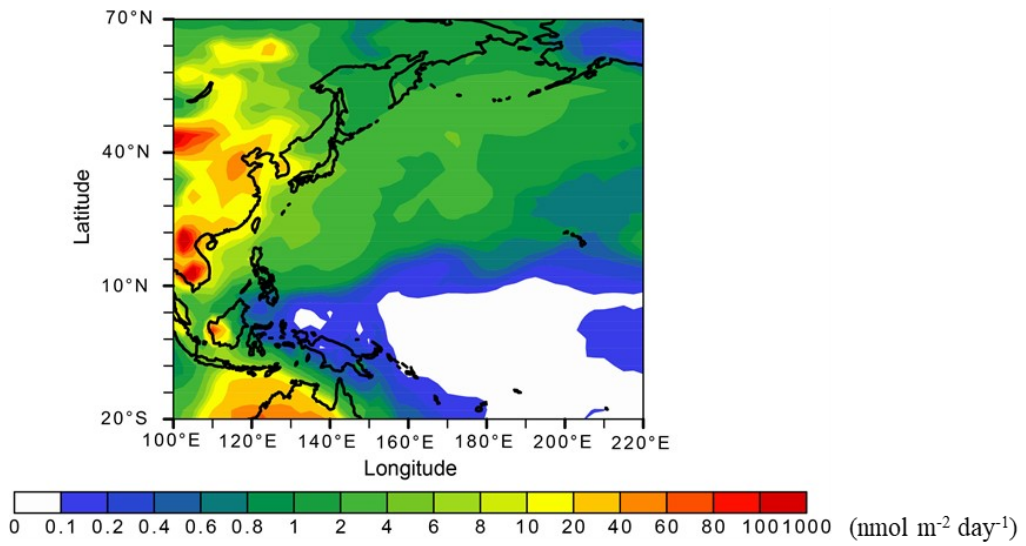
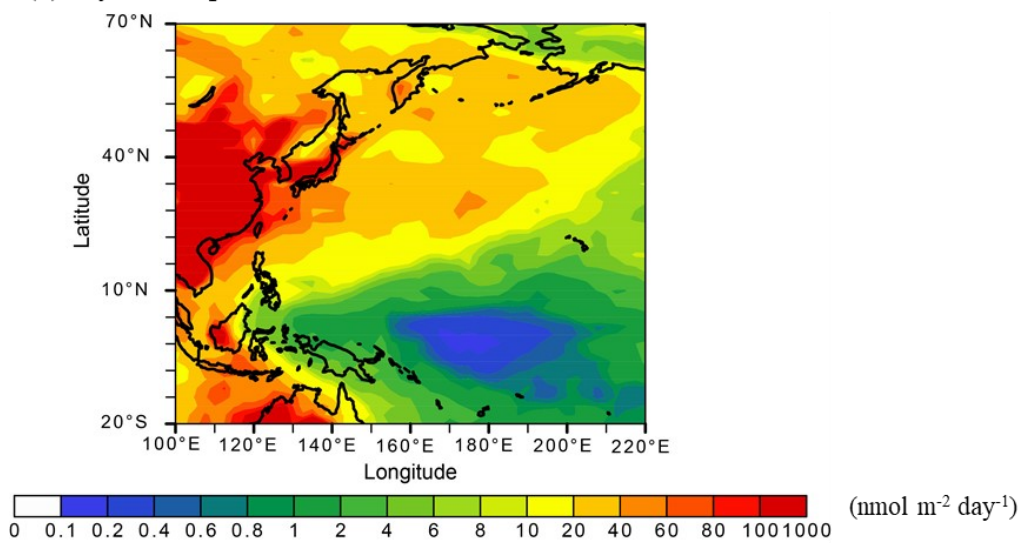


Figure S11. The Fe concentration from each source and size fraction calculated based on (d) the observation and (e) the IMPACT model; Comparison between the model-based estimation and the observation data for (a) the bulk (fine+coarse) Fe concentrations, (b) coarse Fe concentrations, (c) fine Fe concentrations.

(a) Dry deposition



(b) Dry+wet deposition



(c) Dry/(dry+wet) deposition

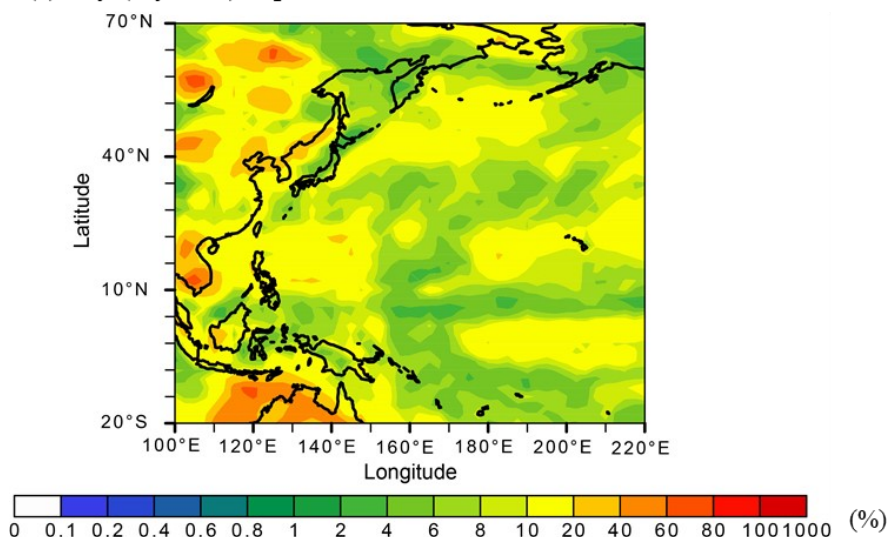


Figure S12. Deposition flux of soluble Fe by (a) dry and (b) dry+wet depositions estimated by the IMPACT model during the group I sampling period. (c) The fraction of dry deposition to the total deposition.

References

- Nishikawa, M., Hao, Q. and Morita, M.: Preparation and evaluation of certified reference materials for Asian mineral dust, *Glob. Environ. Res.*, 4, 103–113, 2000.
- Stein, A. F., Draxler, R. R., Rolph, G. D., Stunder, B. J. B., Cohen, M. D. and Ngan, F.: Noaa's hysplit atmospheric transport and dispersion modeling system, *Bull. Am. Meteorol. Soc.*, 96(February), 2059–2077, doi:10.1175/BAMS-D-14-00110.1, 2015.
- Sun, S.: Behavior of inorganic nitrogen in atmospheric aerosols and its impact on the marine environment in the Pacific Ocean and its marginal waters, M.S. thesis, The University of Tokyo, Chiba, 2017.